The Biochemistry and Theory of Proton Coupled Electron Transfer

Agostino Migliore,[*,†] Nicholas F. Polizzi,[§] Michael J. Therien,[†] David N. Beratan[*,†,§,+]

Departments of Chemistry[†], Biochemistry[§], and Physics[+], Duke University, Durham, NC 27708, USA

1. Figures S1-S9.

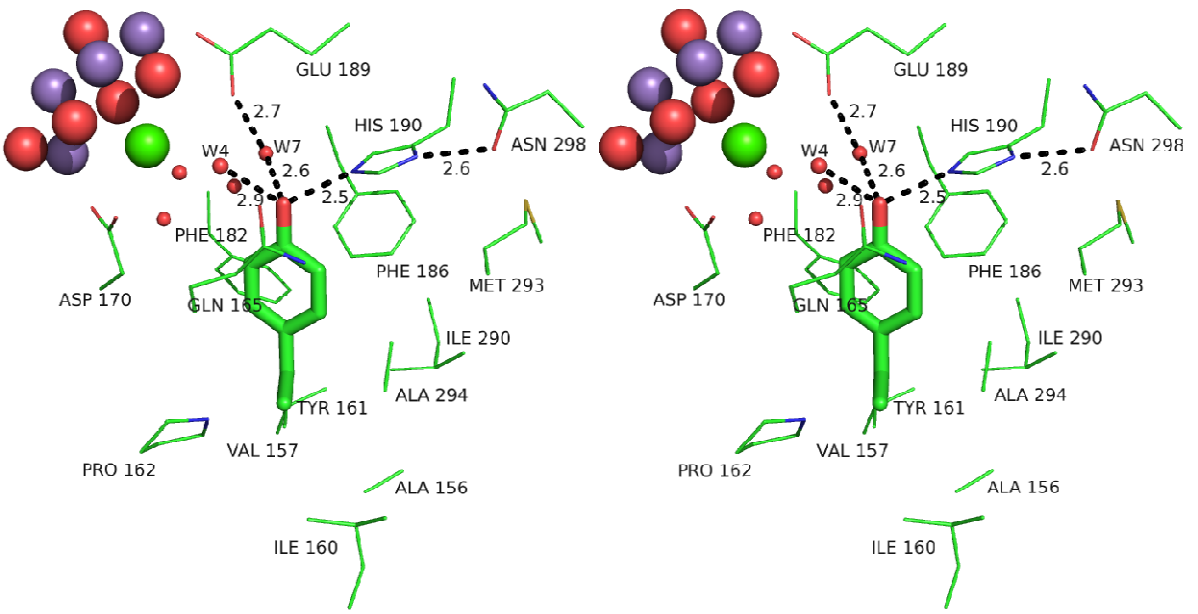

Figure S1. Stereo view of the protein environment surrounding Tyr161 (TyrZ) of Photosystem II from *T. vulcanus* (pdb 3ARC). All amino acid side chains and cofactors within a 5-Å radius

from TyrZ are shown. Distances shown are from the phenolic oxygen of TyrZ to His190 and to crystallographic waters, as well as His190 to Asn298. Crystallographic waters are shown as small red spheres, the WOC as large orange spheres with Mn colored purple, oxygen red and Ca green. Tyr161 is the thick, central amino acid.

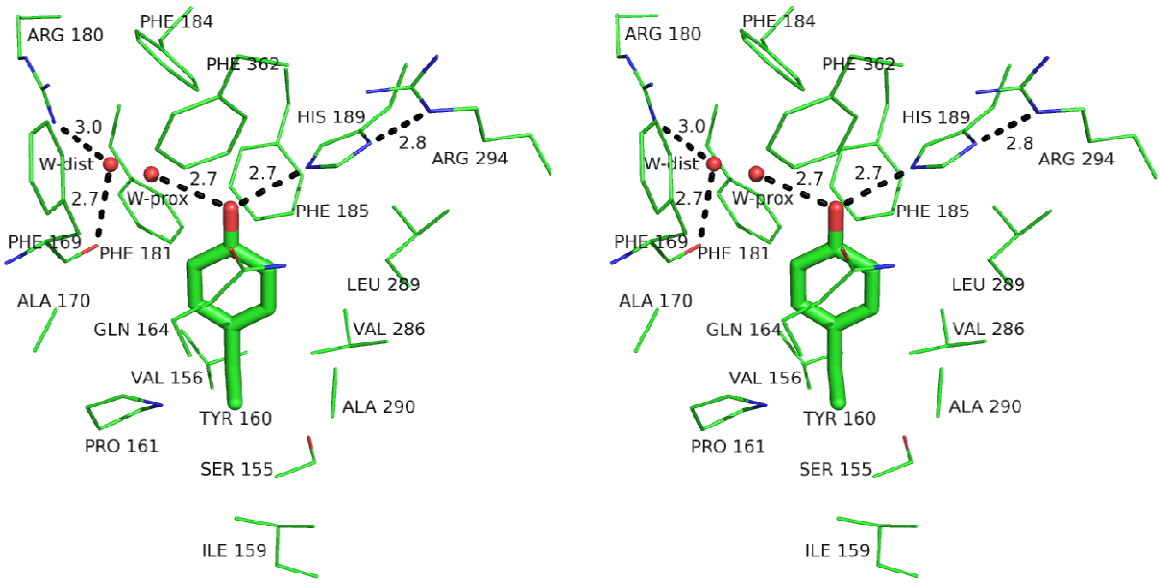

Figure S2. Stereo view of the protein environment surrounding Tyr160 (TyrD) of Photosystem II from *T. vulcanus* (pdb 3ARC). All amino acid sidechains and cofactors within a 5 Å radius of TyrD are shown. Distances shown are from the phenolic oxygen of TyrD to His189 and the "proximal" water, as well as the backbone carbonyl of Phe169 to Arg180, the "distal" water to Arg180, and His189 to Arg294. TyrD is the thick, central amino acid. Waters are shown as red spheres.

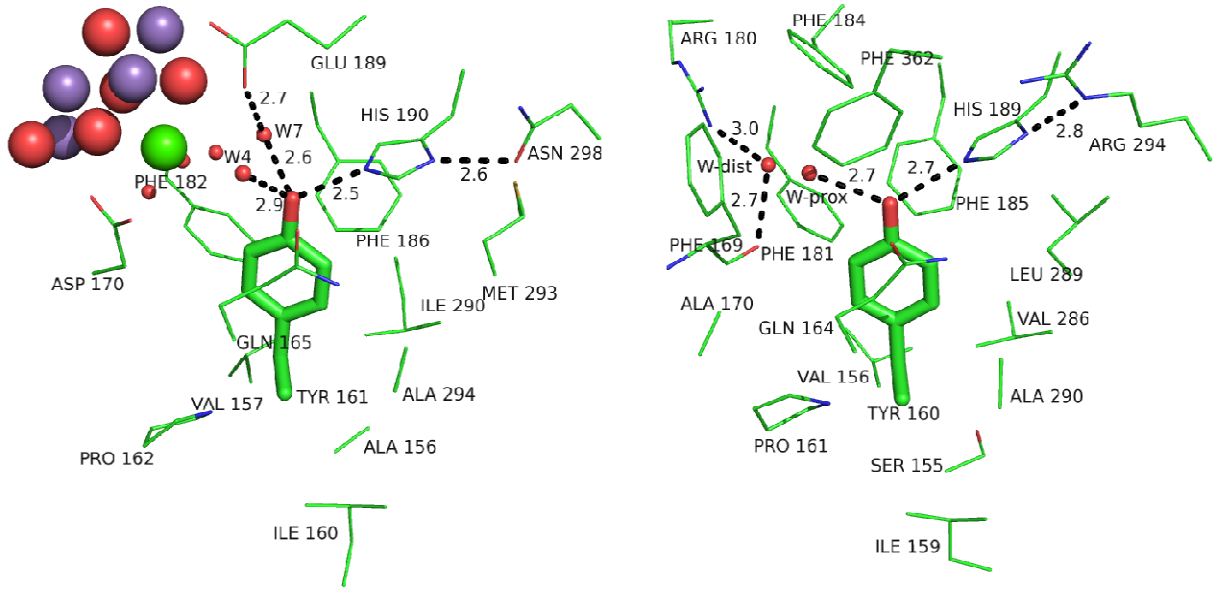

Figure S3. Side by side comparison of the protein environments surrounding D1-Tyr161 (TyrZ) and D2-Tyr160 (TyrD) of Photosystem II from *T. vulcanus* (pdb 3ARC). All amino acid side chains and cofactors within a 5 Å radius from TyrZ are shown. Left: Distances shown are from the phenolic oxygen of TyrZ to His190 and crystallographic waters, as well as His190 to Asn298. Crystallographic waters are shown as small red spheres, the water oxidizing complex as large orange spheres with Mn colored purple, Oxygen red and Ca green. TyrZ is the thick, central amino acid. Right: Distances shown are from the phenolic oxygen of TyrD to His189 and the "proximal" water, as well as the backbone carbonyl of Phe169 to Arg180, the "distal" water to Arg180, and His189 to Arg294. TyrD is the thick, central amino acid.

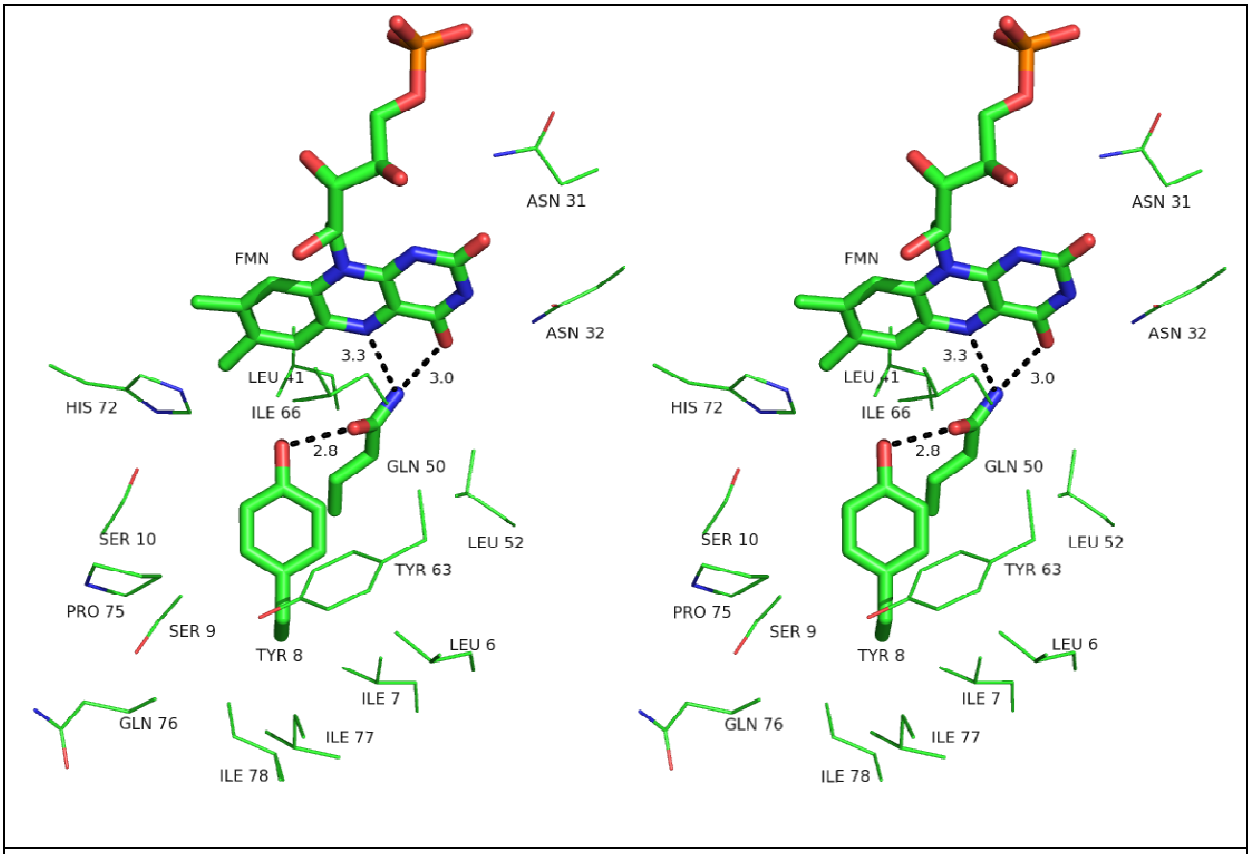

Figure S4. Stereo view of the protein environment surrounding Tyr8 of the BLUF domain from Slr1694 of Synechocystis sp. PCC 6803 (pdb 2HFN). All amino acid side chains and cofactors within a 5 Å radius from Tyr8 are shown. Distances shown are from the phenolic oxygen of Tyr8 to Gln50 or Gln50 to the FMN cofactor.

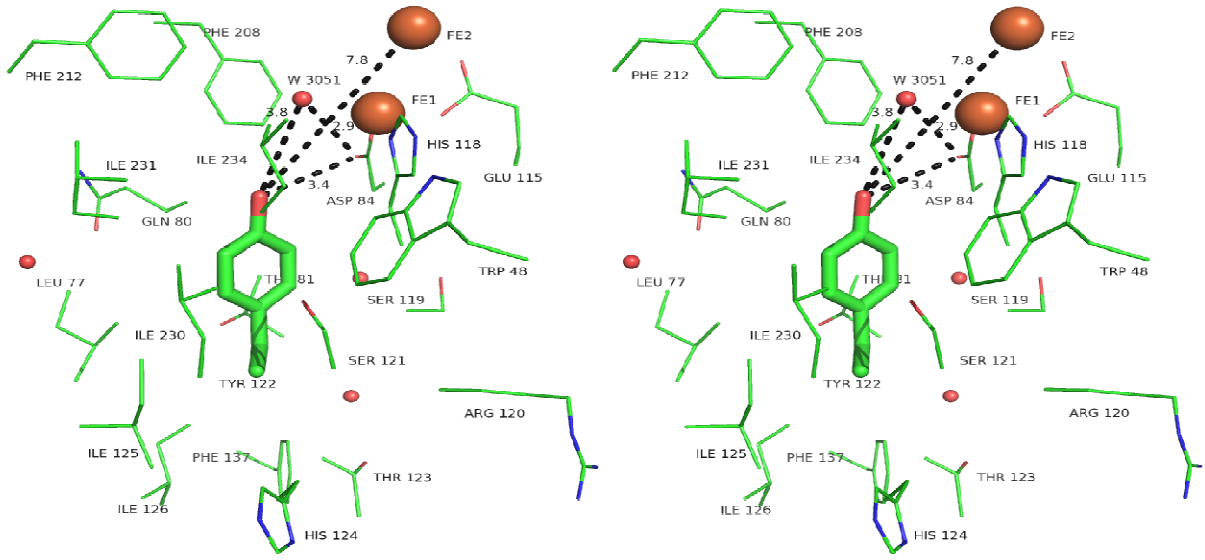

Figure S5. Stereo view of the protein environment surrounding Tyr122 of Ribonucleotide Reductase from *E. coli* (pdb 1MXR). All amino acid side chains and cofactors within a 6 Å radius from Tyr122 are shown, as well as Trp48 and Fe2. Distances shown are from the phenolic oxygen of Tyr122 to ASP84 and a water coordinated to Fe_1 of the diiron active site. Crystallographic waters are shown as small red spheres, the diiron site large orange spheres, and Tyr122 as the thick, central amino acid.

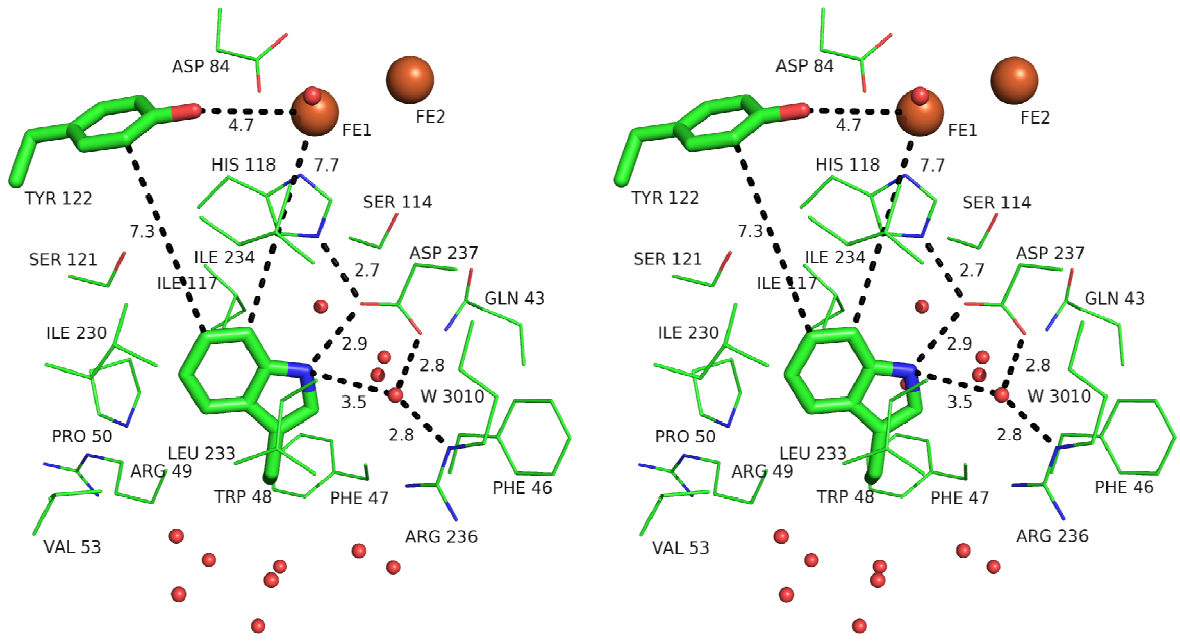

Figure S6. Stereo view of the protein environment surrounding Trp48 of Ribonucleotide Reductase from *E. coli* (pdb 1MXR). All amino acid side chains and cofactors within a 6 Å radius from Trp48 are shown, as well as Tyr122 and Asp84. Crystallographic waters are shown as small red spheres, the diiron site large orange spheres, and Trp48 as the thick, central amino acid.

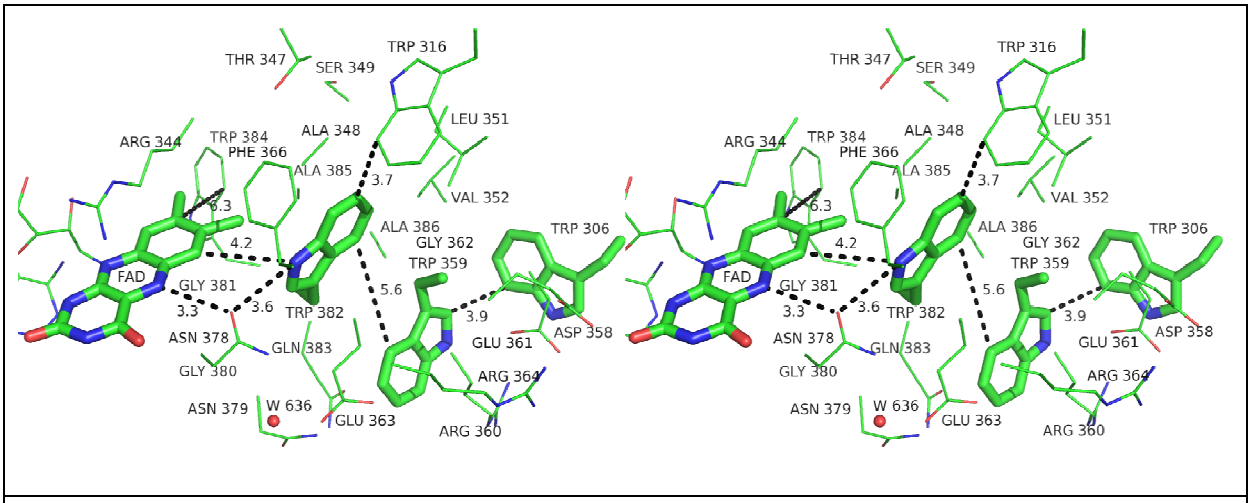

Figure S7. Stereo view of the protein environment surrounding Trp382 of photolyase from *E. coli* (pdb 1DNP). All amino acid side chains and cofactors within a 6 Å radius from Trp382 are shown, as well as Trp306. Crystallographic waters (labeled W) are shown as small red spheres, and Trp382 as the thick, central amino acid. The conserved hole-hopping pathway (including FAD) is rendered with thick lines. Positions of glycine residues are denoted by the label GLY.

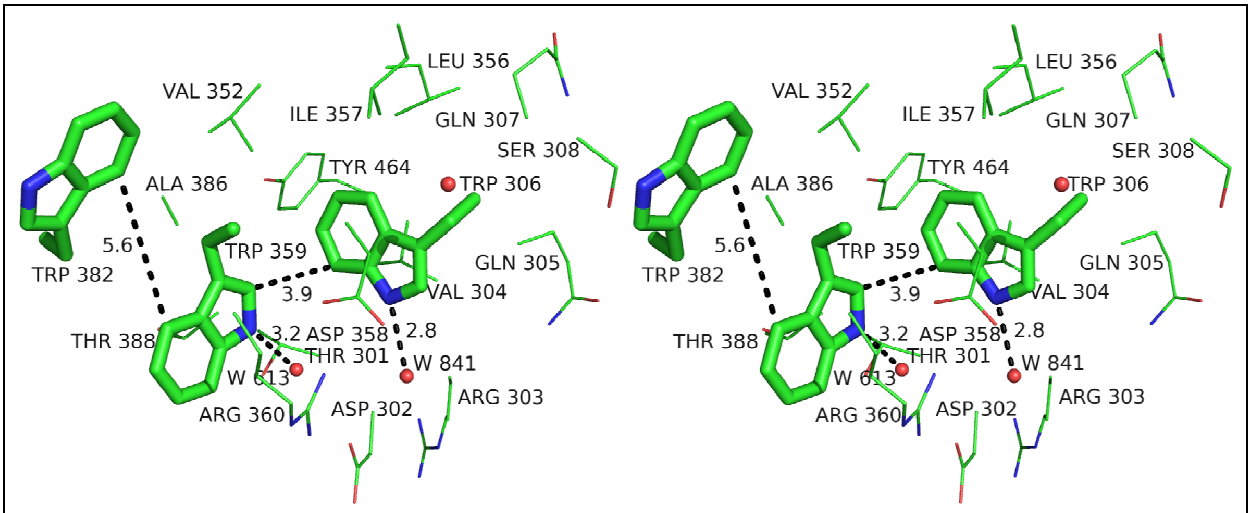

Figure S8. Stereo view of the protein environment surrounding Trp306 of photolyase from *E. coli* (pdb 1DNP). All amino acid side chains and cofactors within a 6 Å radius from Trp306 are shown, as well as Trp382. Crystallographic waters (W) are shown as small red spheres, and Trp306 as the thick, central amino acid. The conserved hole-hopping pathway (excluding FAD) is rendered as thick lines.

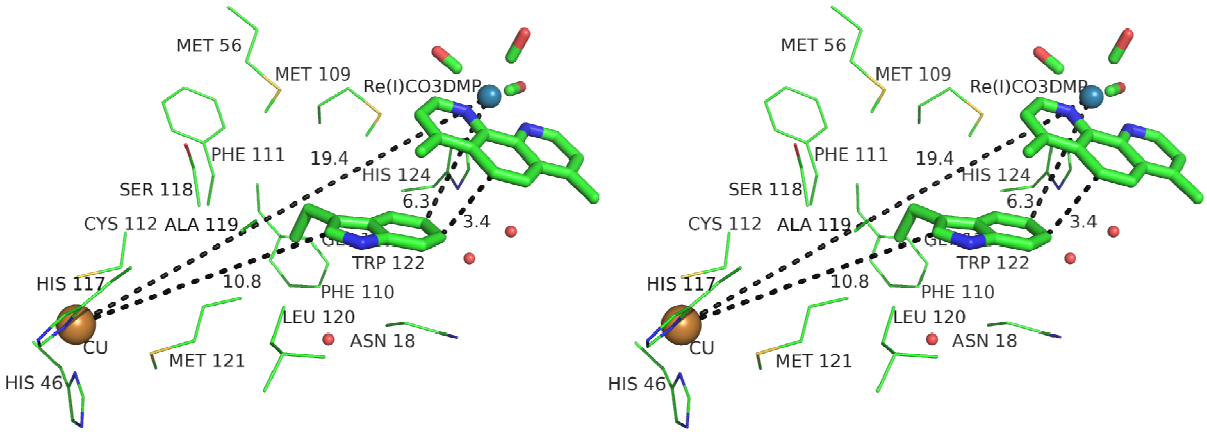

Figure S9. Stereo view of the protein environment surrounding Trp122 of azurin from *Pseudomonas aeruginosa* (pdb 2I7O). All amino acid side chains and cofactors within a 6 Å radius from Trp122 are shown, as well as Cu(I) with its coordinating AAs. Crystallographic waters are shown as small red spheres, and Trp122 as the thick, central AA. $Re^{I}(CO)_3(dmp)$ is also rendered as thick lines, with Re(I) a blue sphere. Distances shown (in Å) correspond to those relevant to hole transfer.

2. Derivation of eqs 5.18 and 5.21.

Consider eq 5.15, which is here rewritten for the electronic state $|\phi_k\rangle$ in vector form:

$$\nabla_Q[\hat{T}_q + V(Q)]|\phi_k\rangle = E_k(Q)|\phi_k\rangle . \tag{S2.1}$$

By applying ∇_Q to eq S2.1 and projecting the resulting equation on the state $|\phi_n\rangle$, it is obtained, similarly to ref [1],

$$\begin{aligned}
&\nabla_Q(\hat{T}_q + V)|\phi_k\rangle = \nabla_Q V|\phi_k\rangle + (\hat{T}_q + V)|\nabla_Q\phi_k\rangle = [\nabla_Q E_k(Q)]|\phi_k\rangle + E_k(Q)|\nabla_Q\phi_k\rangle \\
&\Rightarrow \langle\phi_n|\nabla_Q V|\phi_k\rangle + \langle\phi_n|(\hat{T}_q + V)|\nabla_Q\phi_k\rangle = \langle\phi_n|\nabla_Q V|\phi_k\rangle + E_n(Q)\mathbf{d}_{nk} = E_k(Q)\mathbf{d}_{nk} \qquad \text{(S2.2)} \\
&\Rightarrow \mathbf{d}_{nk} = \frac{\langle\phi_n|\nabla_Q V(Q,q)|\phi_k\rangle}{E_k(Q) - E_n(Q)}
\end{aligned}$$

The orthonormality of the basis electronic wave functions at any given nuclear coordinate gives

$$\left\langle \phi_n \middle| \phi_j \right\rangle = \delta_{nj} \;\forall Q \;\Rightarrow\; \nabla_Q \left\langle \phi_n \middle| \phi_j \right\rangle = \left\langle \nabla_Q \phi_n \middle| \phi_j \right\rangle + \left\langle \phi_n \middle| \nabla_Q \phi_j \right\rangle \;\Rightarrow\; \left\langle \nabla_Q \phi_n \middle| \phi_j \right\rangle = -\left\langle \phi_n \middle| \nabla_Q \phi_j \right\rangle \quad \text{(S2.3)}$$

Proceeding as in ref 1 and using eq S2.3, we obtain

$$\begin{aligned} \left\langle \phi_n \middle| \nabla_Q^2 \middle| \phi_k \right\rangle &= \nabla_Q \cdot \left\langle \phi_n \middle| \nabla_Q \phi_k \right\rangle - \left\langle \nabla_Q \phi_n \middle| \nabla_Q \phi_k \right\rangle = \nabla_Q \cdot \mathbf{d}_{nk} - \sum_j \left\langle \nabla_Q \phi_n \middle| \phi_j \right\rangle \cdot \left\langle \phi_j \middle| \nabla_Q \phi_k \right\rangle \\ &= \nabla_Q \cdot \mathbf{d}_{nk} + \sum_j \left\langle \phi_n \middle| \nabla_Q \phi_j \right\rangle \cdot \left\langle \phi_j \middle| \nabla_Q \phi_k \right\rangle = \nabla_Q \cdot \mathbf{d}_{nk} + \sum_j \mathbf{d}_{nj} \cdot \mathbf{d}_{jk} \end{aligned} \quad \text{(S2.4)}$$

that is eq 5.21 in the paper.

3. Derivation of eqs 6.9 and 6.10.

Consider the self-exchange (weak-overlap) ET reactions

$$\mathrm{Ox}_n + \mathrm{Red}_n \rightleftharpoons \mathrm{Red}_n + \mathrm{Ox}_n \quad (n = 1, 2) \quad \text{(S3.1)}$$

and the cross-reaction

$$\mathrm{Ox}_1 + \mathrm{Red}_2 \rightleftharpoons \mathrm{Red}_1 + \mathrm{Ox}_2 \quad \text{(S3.2)}$$

The following approximation is used for the reorganization energy of the cross-reaction: [2, 3]

$$\lambda = \lambda_{12} = \lambda_{21} = \frac{\lambda_{11} + \lambda_{22}}{2} \quad \text{(S3.3)}$$

The rate constants k_{12} and k_{21} for the forward and backward reactions in eq S3.2 are related by

$$K_{12} = \frac{k_{12}}{k_{21}} \quad \text{(S3.4)}$$

where K_{12} is the equilibrium constant for the ET cross-reaction. The expression of k_{12} is

$$k_{12} = \kappa_{\mathrm{el}} Z \exp\left(-\frac{\Delta G^*}{k_{\mathrm{B}} T} \right). \tag{S3.5}$$

(see eq 6.7 and the meaning of the symbols in the article). For a self-exchange reaction, $\Delta G^0 = 0$ and $w^p = w^r$, so that $\Delta G_0^R = 0$ and, considering eqs 6.8a-b, eq S3.5 becomes

$$k_{nn} = (\kappa_{\mathrm{el}})_{nn} Z \exp\left(-\frac{w_{nn}}{k_{\mathrm{B}} T} \right) \exp\left(-\frac{\lambda_{nn}}{4 k_{\mathrm{B}} T} \right), \qquad n = 1, 2. \tag{S3.6}$$

Therefore, for $Z = (Z_{11} Z_{22})^{1/2}$, $\kappa_{\mathrm{el}} = \left[(\kappa_{\mathrm{el}})_{11} (\kappa_{\mathrm{el}})_{22} \right]^{1/2}$, and using eq S3.3, it is

$$\ln\left[\frac{k_{11} k_{22}}{Z^2 (\kappa_{\mathrm{el}})_{11} (\kappa_{\mathrm{el}})_{22}} \right] = -\frac{w_{11} + w_{22}}{k_{\mathrm{B}} T} - \frac{\lambda_{11} + \lambda_{22}}{4 k_{\mathrm{B}} T} = -\frac{\lambda}{2 k_{\mathrm{B}} T}. \tag{S3.7}$$

It is also

$$\begin{aligned}
\ln\left(\frac{k_{12} k_{21}}{Z^2 \kappa_{\mathrm{el}}^2} \right) &= -\frac{w^r + w^p}{k_{\mathrm{B}} T} - \frac{(\lambda + \Delta G^0 + w^p - w^r)^2 + (\lambda - \Delta G^0 + w^r - w^p)^2}{4 \lambda k_{\mathrm{B}} T} \\
&= -\frac{w^r + w^p}{k_{\mathrm{B}} T} - \frac{\lambda}{2 k_{\mathrm{B}} T} - \frac{(\Delta G^0 + w^p - w^r)^2}{2 \lambda k_{\mathrm{B}} T} \\
&= -2 \frac{w^r + w^p - w_{11} - w_{22}}{2 k_{\mathrm{B}} T} + \ln\left[\frac{k_{11} k_{22}}{Z^2 (\kappa_{\mathrm{el}})_{11} (\kappa_{\mathrm{el}})_{22}} \right] - \frac{(\Delta G^0 + w^p - w^r)^2}{2 \lambda k_{\mathrm{B}} T} \\
&= \ln W_{12}^2 + \ln\left[\frac{k_{11} k_{22}}{Z^2 (\kappa_{\mathrm{el}})_{11} (\kappa_{\mathrm{el}})_{22}} \right] + \ln\left\{ \exp\left[-\frac{(\Delta G^0 + w^p - w^r)^2}{2 \lambda k_{\mathrm{B}} T} \right] \right\} \\
&= \ln\left\{ \frac{k_{11} k_{22}}{Z^2 (\kappa_{\mathrm{el}})_{11} (\kappa_{\mathrm{el}})_{22}} W_{12}^2 \exp\left[-\frac{(\Delta G^0 + w^p - w^r)^2}{2 \lambda k_{\mathrm{B}} T} \right] \right\}
\end{aligned} \tag{S3.8}$$

whence, by exploiting eq S3.4,

$$
\begin{aligned}
& k_{12}\,k_{21} = \kappa_{\mathrm{el}}^2 \frac{k_{11}\,k_{22}\,f_{12}}{(\kappa_{\mathrm{el}})_{11}(\kappa_{\mathrm{el}})_{22}} W_{12}^2 \\
& \Rightarrow\; k_{12}^2 = \kappa_{\mathrm{el}}^2 \frac{k_{11}\,k_{22}\,k_{12}\,f_{12}}{(\kappa_{\mathrm{el}})_{11}(\kappa_{\mathrm{el}})_{22}\,k_{21}} W_{12}^2 = \kappa_{\mathrm{el}}^2 \frac{k_{11}\,k_{22}\,K_{12}\,f_{12}}{(\kappa_{\mathrm{el}})_{11}(\kappa_{\mathrm{el}})_{22}} W_{12}^2 \\
& \Rightarrow k_{12} = \kappa_{\mathrm{el}} \left[\frac{k_{11}\,k_{22}\,K_{12} f_{12}}{(\kappa_{\mathrm{el}})_{11}(\kappa_{\mathrm{el}})_{22}} \right]^{1/2} W_{12}
\end{aligned}
\tag{S3.9}
$$

that is eq 6.9 for

$$
\ln f_{12} = -\frac{(\Delta G^0 + w^p - w^r)^2}{2\lambda k_{\mathrm{B}} T}. \tag{S3.10}
$$

Eq S3.10 is the first equality in eq 6.10. The second equality in eq 6.10, which generalizes the second equality in eq 6.6, is then easily verified. In fact,

$$
\begin{aligned}
& \ln K_{12} = \ln\left(\frac{k_{12}}{k_{21}}\right) = \frac{w^p - w^r}{k_{\mathrm{B}} T} + \frac{(\lambda - \Delta G^0 + w^r - w^p)^2 - (\lambda + \Delta G^0 + w^p - w^r)^2}{4\lambda k_{\mathrm{B}} T} \\
& = \frac{w^p - w^r}{k_{\mathrm{B}} T} - \frac{\Delta G^0 + w^p - w^r}{k_{\mathrm{B}} T}
\end{aligned}
\tag{S3.11}
$$

so that

$$
\ln K_{12} + \frac{w^r - w^p}{k_B T} = -\frac{\Delta G^0 + w^p - w^r}{k_{\mathrm{B}} T}. \tag{S3.12}
$$

Moreover, eq S3.7 yields

$$
\ln\left[\frac{k_{11}\,k_{22}}{Z^2 (\kappa_{\mathrm{el}})_{11}(\kappa_{\mathrm{el}})_{22}}\right] + \frac{w_{11} + w_{22}}{k_{\mathrm{B}} T} = -\frac{\lambda}{2 k_{\mathrm{B}} T}. \tag{S3.13}
$$

Finally, eqs S3.12 and S3.13 give

$$\frac{1}{4}\frac{\left(\ln K_{12}+\frac{w^r-w^p}{k_BT}\right)^2}{\ln\left[\frac{k_{11}k_{22}}{Z^2(\kappa_{\mathrm{el}})_{11}(\kappa_{\mathrm{el}})_{22}}\right]+\frac{w_{11}+w_{22}}{k_BT}}=-\frac{(\Delta G^0+w^p-w^r)^2}{2\lambda k_{\mathrm{B}}T}=\ln f_{12} \tag{S3.14}$$

quod erat demonstrandum.

As an alternative, one can proceed directly via manipulation of eq S3.8.

4. Derivation of eq B5.

Averaging both sides of eq B4 over state $|\phi_n,R,Q\rangle$, one obtains:

$$\begin{aligned}
&i\hbar\frac{\partial}{\partial t}\rho_{nn}(R,Q,t)=\langle\phi_n,R,Q|\left(\frac{P_R^2+P_Q^2}{2}+H\right)\hat{\rho}(t)-\hat{\rho}(t)\left(\frac{P_R^2+P_Q^2}{2}+H\right)|\phi_n,R,Q\rangle\\
&=\sum_{\mu,\nu}c_\mu(t)c_\nu^*(t)\int dR'dQ'dR''dQ''\chi_\mu^p(R')\chi_\mu(Q')\chi_\nu^p(R'')\chi_\nu(Q'')\left\{\tfrac{1}{2}\delta_{n\mu}\delta_{\nu n}\right.\\
&\times\left[\langle R,Q|\left(P_R^2+P_Q^2\right)|R',Q'\rangle\langle R'',Q''|R,Q\rangle-\langle R,Q|R',Q'\rangle\langle R'',Q''|\left(P_R^2+P_Q^2\right)|R,Q\rangle\right]\\
&\left.+\langle R,Q|R',Q'\rangle\langle R'',Q''|R,Q\rangle\left[V_{n\mu}(R,Q)\delta_{\nu n}-V_{\nu n}(R,Q)\delta_{n\mu}\right]\right\}\\
&=-\frac{\hbar^2}{2}|c_n(t)|^2\int dR'dQ'dR''dQ''\chi_n^p(R')\chi_n(Q')\chi_n^p(R'')\chi_n(Q'')\\
&\times\left[\delta(R''-R)\delta(Q''-Q)\delta^{(2)}(R-R')\delta^{(2)}(Q-Q')-\delta(R-R')\delta(Q-Q')\delta^{(2)}(R''-R)\delta^{(2)}(Q''-Q)\right]\\
&+\sum_k\int dR'dQ'dR''dQ''\delta(R-R')\delta(Q-Q')\delta(R''-R)\delta(Q''-Q)\left[\chi_k^p(R')\chi_k(Q')\chi_n^p(R'')\chi_n(Q'')\right.\\
&\left.c_k(t)c_n^*(t)V_{nk}(R,Q)-\chi_n^p(R')\chi_n(Q')\chi_k^p(R'')\chi_k(Q'')c_k^*(t)c_n(t)V_{kn}(R,Q)\right]
\end{aligned} \tag{S4.1}$$

where P_X is the momentum operator for the mass-weighted coordinates X = R, Q, and we exploited the orthogonality of the basis sets for electronic state and proton-solvent position representation. At this point, use of the following property of the Dirac delta function and its derivatives[4]

$$\int_{-\infty}^{+\infty} \delta^{(n)}(x - x_0) f(x) dx = (-1)^n f^{(n)}(x_0) \tag{S4.2}$$

yields zero for the first integral. Since $V_{nk} = V_{kn}$ for the given Hamiltonian and real wave functions, eq B5 is soon obtained:

$$\begin{aligned} i\hbar \frac{\partial}{\partial t} \rho_{nn}(R,Q,t) &= \sum_k V_{nk}(R,Q)[c_k(t)c_n^*(t) - c_k^*(t)c_n(t)]\chi_k^p(R)\chi_k(Q)\chi_n^p(R)\chi_n(Q) \\ &= 2i\sum_{k\neq n} V_{nk}(R,Q)\,\mathrm{Im}[c_k(t)c_n^*(t)\chi_k^p(R)\chi_k(Q)\chi_n^p(R)\chi_n(Q)] \end{aligned} \tag{S4.3}$$

References and Notes

(1) Hobey, W. D.; McLachlan, A. D. *J. Chem. Phys.* **1960**, *33*, 1695.
(2) Marcus, R. A. *J. Phys. Chem.* **1963**, *67*, 853.
(3) Marcus, R. A. *J. Phys. Chem.* **1968**, *72*, 891.
(4) Cohen-Tannoudji, C.; Diu, B.; Laloë, F. *Quantum Mechanics*; Hermann: Paris, 1977.